第29卷　第6期　　　　材　料　研　究　学　报　　　　Vol. 29 No. 6
2015 年 6 月　　　　CHINESE JOURNAL OF MATERIALS RESEARCH　　　　June 2015

$(Y_{0.08}Sr_{0.92})_{1-x}Ti_{0.6}Fe_{0.4}O_{3-\delta}$混合导体材料的电子-离子阻抗特性*

单　科[1]　郭兴敏[2]

1. 红河学院理学院 新能源材料重点实验室　蒙自　661199
2. 北京科技大学钢铁冶金新技术国家重点实验室　北京 100083

摘 要 用溶胶-凝胶法制备了$(Y_{0.08}Sr_{0.92})_{1-x}Ti_{0.6}Fe_{0.4}O_{3-\delta}$($x$ = 0.05, 0.07, 0.10)混合导体材料, 用X射线衍射(XRD)分析该材料的物相, 用交流阻抗法和电子阻塞电极法分别测定材料的总电导率与离子电导率, 研究了A位缺位对$(Y_{0.08}Sr_{0.92})_{1-x}Ti_{0.6}Fe_{0.4}O_{3-\delta}$混合导体材料的结构、电性能及阻抗行为的影响。结果表明, 所有试样都具有单一立方相钙钛矿结构; 在测试温度范围内$(Y_{0.08}Sr_{0.92})_{1-x}Ti_{0.6}Fe_{0.4}O_{3-\delta}$($x$ = 0.05, 0.07, 0.10)的总电导率随着温度的升高先增大后减小, 表现为小极化子导电机理; 随着A位缺位量的增加, 总电导率降低。$(Y_{0.08}Sr_{0.92})_{1-x}Ti_{0.6}Fe_{0.4}O_{3-\delta}$($x$=0.05, 0.07, 0.10)在800℃的总电导率为0.011−0.26 S•cm^{-1}。$(Y_{0.08}Sr_{0.92})_{1-x}Ti_{0.6}Fe_{0.4}O_{3-\delta}$的总电导率阻抗谱只显示了高频斜线部分, 说明材料主要以电子电导为主; 离子传导的弛豫时间逐渐随着A位缺位量的增加而增大, 说明A位缺位不利于离子在晶界中的传导。

关键词 无机非金属材料, $(Y_{0.08}Sr_{0.92})_{1-x}Ti_{0.6}Fe_{0.4}O_{3-\delta}$, 电子阻抗, 离子阻抗, 弛豫

分类号 TB321, TQ174　　　　文章编号　1005-3093(2015)06-0429-05

Electronic-ionic Impedance Characteristics of $(Y_{0.08}Sr_{0.92})_{1-x}Ti_{0.6}Fe_{0.4}O_{3-\delta}$ Mixed Conductor

SHAN Ke[1**]　GUO Xingmin[2]

1. Laboratory of New Materials for Power Sources, College of Science, Honghe University, Mengzi 661199, China
2. State Key Laboratory of Advanced Metallurgy, University of Science and Technology Beijing, Beijing 100083, China

*Supported by National Natural Science Foundation of China No. 51374017.

Manuscript received November 13, 2014; in revised form December 23, 2014.

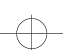
**To whom correspondence should be addressed, Tel: 13691055859, E-mail: shankekeshan@163.com

ABSTRACT A single phase A-site-deficient perovskite $(Y_{0.08}Sr_{0.92})_{1-x}Ti_{0.6}Fe_{0.4}O_{3-\delta}$ (x=0.05, 0.07, 0.10) was synthesized at 1350 °C in air by sol-gel method. The effect of A-site deficiency in $(Y_{0.08}Sr_{0.92})_{1-x}Ti_{0.6}Fe_{0.4}O_{3-\delta}$ on its phase structure, electrical and ionic conductivity and impedance was investigated. The partial oxygen ionic conductivity decreases with the increasing A-site deficiency, which may be attributed to the tendency for oxygen vacancy ordering. The n-type electronic conductivity in air increases with the increasing A-site deficiency, which may be attributed to the decrease of $[Fe_{Ti}^{'}]$ and $[h^{\cdot}]$ due to the possible ionization reaction of ferric iron. The total electrical conductivity of $(Y_{0.08}Sr_{0.92})_{1-x}Ti_{0.6}Fe_{0.4}O_{3-\delta}$ (x=0.05, 0.07, 0.10) varies from 0.11 S•cm^{-1} to 0.26 S•cm^{-1} at 800°C. Only one oblique line in high frequency range for each temperature is presented, demonstrating that the electronic conductivity should mainly contribute to the total electrical conductivity. The increase of A-site deficiency is unfavorable for ion conductivity due to a subsequently rising relaxation time.

KEY WORDS inorganic non-metallic materials, $(Y_{0.08}Sr_{0.92})_{1-x}Ti_{0.6}Fe_{0.4}O_{3-\delta}$, electrical impedance, ionic impedance, relaxation

ABO_3钙钛矿结构的$SrTiO_3$在很宽的氧分压和温度范围内保持结构和性能的稳定, 在燃料电池、氧传感器和透氧膜中有良好的应用前景[1-4]。虽然化学计量比的$SrTiO_3$电导率很低, 但是其在A位和B位都有很强的掺杂能力, 因而可进行掺杂对其改性。掺杂的$SrTiO_3$表现出混合导体的性质, 同时具有氧离子导电[5-11]和电子导电性能[12-15], 不仅具有催化活

* 国家自然科学基金51374017资助项目。
2014年11月13日收到初稿; 2014年12月23日收到修改稿。
本文联系人: 单　科



性, 在中高温下还能够选择性透氧。同时, $SrTiO_3$全陶瓷部件在高温下具有更高的结构稳定性和化学稳定性。掺杂的$SrTiO_3$有很高的电导性能, 并能与多种电解质材料兼容, 不会发生物理和化学反应。通过A、B位的共掺杂, 还可调节和控制材料的热膨胀系数。

在理想的ABO_3钙钛矿结构中A、B位元素是等量的, 但是实际上A、B位元素是可以不等量的。Y, Fe共掺杂的$SrTiO_3$($Y_{0.06}Sr_{0.94}Ti_{0.6}Fe_{0.4}O_{3-\delta}$)具有较高的电子电导率和离子电导率[16], 本文研究A位缺位量对其晶格结构、致密化、电性能以及阻抗行为的影响。

1 实验方法

1.1 $(Y_{0.08}Sr_{0.92})_{1-x}Ti_{0.6}Fe_{0.4}O_{3-\delta}$的制备

以分析纯的醋酸锶($Sr(CH_3COO)_2\cdot 2H_2O$), 钛酸四丁酯($Ti(CH_3CH_2CH_2CH_2O)_4$)氧化钇(Y_2O_3)和三氧化二铁(Fe_2O_3)为原料, 用溶胶-凝胶法合成A位缺位的$(Y_{0.08}Sr_{0.92})_{1-x}Ti_{0.6}Fe_{0.4}O_{3-\delta}$($x$=0.05, 0.07, 0.10)[16]。将在1100℃预烧10 h, 然后将其用50 Mpa的单轴压力干压成圆片, 在1350℃保温烧结5 h, 得到$(Y_{0.08}Sr_{0.92})_{1-x}$-$Ti_{0.6}Fe_{0.4}O_{3-\delta}$。

1.2 材料的表征

用D/max-A型转靶X射线衍射仪分析粉末的物相。测试条件: 工作电压40 kV, 工作电流40 mA, 使用Cu-$K\alpha$辐射, 连续扫描方式, 步长为0.02°, 扫描范围为10~90°。用Quanta FEG 650扫描电镜观察样品断面的形貌。

使用电化学CHI660B工作站测试电导率, 在频率范围0.01−10^5 Hz内, 测试样品的阻抗谱。先用铂浆将样品的2个表面涂覆均匀, 再粘上铂丝后, 在800℃煅烧30 min即可得到薄膜电极, 用于电导率的测量。用电子阻塞电极的方法测量离子电导率[17]。YSZ是纯氧离子导体, 因此将其作为电子阻塞电极的电解质片。将烧结好的试样片一面均匀涂满铂浆, 粘贴在YSZ片上。再将贴好的复合片放入管式炉中, 在800℃煅烧30 min, 再将烧好后的样品的边缘用玻璃体密封, 将样品的边缘与空气完全隔离, 使两薄片接界处的缝隙完全封闭。最后将试样/YSZ复合片两面均涂上铂浆层, 粘上铂丝, 在800℃烧结30 min, 即得到待测试样。

2 结果和讨论

2.1 $(Y_{0.08}Sr_{0.92})_{1-x}Ti_{0.6}Fe_{0.4}O_{3-\delta}$的结构和形貌

图1给出了$(Y_{0.08}Sr_{0.92})_{1-x}Ti_{0.6}Fe_{0.4}O_{3-\delta}$($x$=0.05, 0.07, 0.10) 在1350℃烧结5 h的XRD图。由图1可以看出, 所有的样品表现出单一的钙钛矿结构, 没有杂质峰, 说明Y和Fe共掺杂并没有影响$SrTiO_3$的钙钛矿结构。

钙钛矿的结构类型, 通常由容差因子

$$t=(r_A+r_O)\Big/\sqrt{2}(r_B+r_O) \qquad (1)$$

确定, 式中r_A, r_B和r_O分别为A位, B位不同元素的平均离子半径和氧离子半径; 理想的立方相钙钛矿结构的容差因子t=1, 当0.95＜t＜1.04时, 材料可保持理想的立方钙钛矿结构。当0.90＜t＜1时钙钛矿结构可稳定存在, 当0.75＜t＜0.9时钙钛矿为正交结构。根据离子半径, 用式1可计算出$(Y_{0.08}Sr_{0.92})_{1-x}Ti_{0.6}Fe_{0.4}O_{3-\delta}$($x$=0.05, 0.07, 0.10)的容差因子为0.9298-0.9544, 如图2所示, 说明$(Y_{0.08}Sr_{0.92})_{1-x}Ti_{0.6}Fe_{0.4}O_{3-\delta}$($x$=0.05, 0.07, 0.10)的立方相的钙钛矿结构能够稳定存在; 随着A

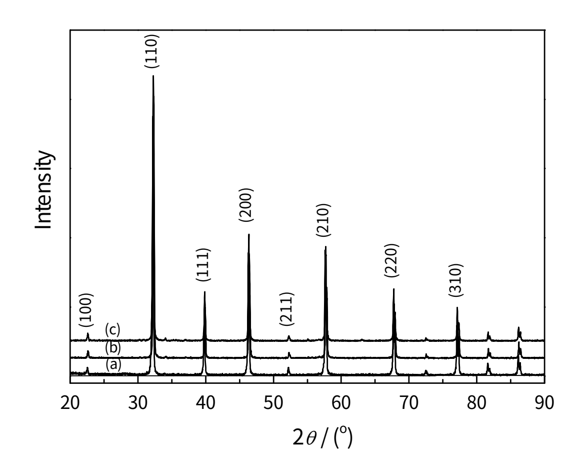


图1 $(Y_{0.08}Sr_{0.92})_{1-x}Ti_{0.6}Fe_{0.4}O_{3-\delta}$在1350℃烧结5 h的XRD图谱

Fig.1 X-ray diffraction patterns of (a) $(Y_{0.08}Sr_{0.92})_{0.95}Ti_{0.6}Fe_{0.4}$-$O_{3-\delta}$, (b) $(Y_{0.08}Sr_{0.92})_{0.93}Ti_{0.6}Fe_{0.4}O_{3-\delta}$ and (c) $(Y_{0.08}Sr_{0.92})_{0.90}$-$Ti_{0.6}Fe_{0.4}O_{3-\delta}$ sintered at 1350ºC in air for 5 h and indexed with cubic indices

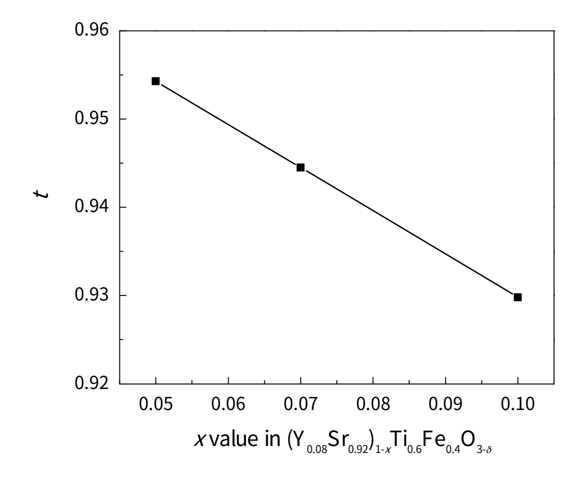


图2 $(Y_{0.08}Sr_{0.92})_{1-x}Ti_{0.6}Fe_{0.4}O_{3-\delta}$ (x= 0.05, 0.07, 0.10)容差因子随x值变化曲线

Fig.2 Relation diagram of the tolerance factor and A-site deficiency for $(Y_{0.08}Sr_{0.92})_{1-x}Ti_{0.6}Fe_{0.4}O_{3-\delta}$

位缺位量的增大容差因子呈减小趋势, 表明A为缺位导致立方钙钛矿的晶格的扭曲程度增大。

图3为1350℃下烧结的$(Y_{0.08}Sr_{0.92})_{1-x}Ti_{0.6}Fe_{0.4}O_{3-\delta}$样品表面的SEM图。可以看出, 随着A位缺位量的增加, 样品的气孔明显增大, 烧结的致密度降低, 这表明A位缺位不利于$(Y_{0.08}Sr_{0.92})_{1-x}Ti_{0.6}Fe_{0.4}O_{3-\delta}$的致密化过程。

2.2 材料的电性能

2.2.1 *总电导率和阻抗行为*　图4给出了$(Y_{0.08}Sr_{0.92})_{1-x}Ti_{0.6}Fe_{0.4}O_{3-\delta}$的复阻抗谱图。可以看出, 图4只显示高频斜线部分, 说明对材料电导率产生贡献的主要是电子电导; 随着温度的升高材料阻抗随之降低, 随着缺位量的增加材料的阻抗却增大。

图5给出了$(Y_{0.08}Sr_{0.92})_{1-x}Ti_{0.6}Fe_{0.4}O_{3-\delta}$样品的电导率在400−900℃范围大气气氛中电导率随温度变化图。由图5可知, 样品的电导率随温度的升高先增大, 达到最大值后随着温度的升高而减小, 表现为小极化子导电机理, 材料为n型导电。在很多混合导体材料中都可观察到这一规律[18, 19]; 样品的电导率随着A位缺位量的增加而降低, 可能是Fe^{3+}的离子化导致了电子空穴浓度的降低(式(2))[7], 从而导致样品的电导率随A位缺位量的增加而降低$(Y_{0.08}Sr_{0.92})_{0.95}$-$Ti_{0.6}Fe_{0.4}O_{3-\delta}$在800℃的电导率为0.162 S•cm^{-1}。

$$(Fe^{3+})'_{Ti} + h^{\cdot} \leftrightarrow (Fe^{4+})^{x}_{Ti} \tag{2}$$

2.2.2 *离子电导率及其阻抗行为的研究*　图6给出了$(Y_{0.08}Sr_{0.92})_{0.90}Ti_{0.6}Fe_{0.4}O_{3-\delta}$在不同温度下离子传导的复阻抗谱图。由图6a可以看出, 温度较低时阻抗谱表现出一个半圆, 随着温度的升高半圆越来越小。半圆与横轴相交, 截距随着温度的升高逐渐减小; 当温度较高时, 出现两个半圆。由图6b(等效电路图见图6b插图)可知, 半圆与横轴相交的截距代表样品的晶粒阻抗, 中频区的弧段代表样品的晶界阻抗, 低频区出现的弧段代表了样品/电极的界面阻抗。由此可见, 样品内传导由氧离子在晶界上的弛豫过程主导。

图7给出了$(Y_{0.08}Sr_{0.92})_{1-x}Ti_{0.6}Fe_{0.4}O_{3-\delta}$在离子传导测试中的虚部与频率的关系曲线。可以看出, 都只存在一个最高峰, 对应试样的晶界阻抗, 只有一个晶界

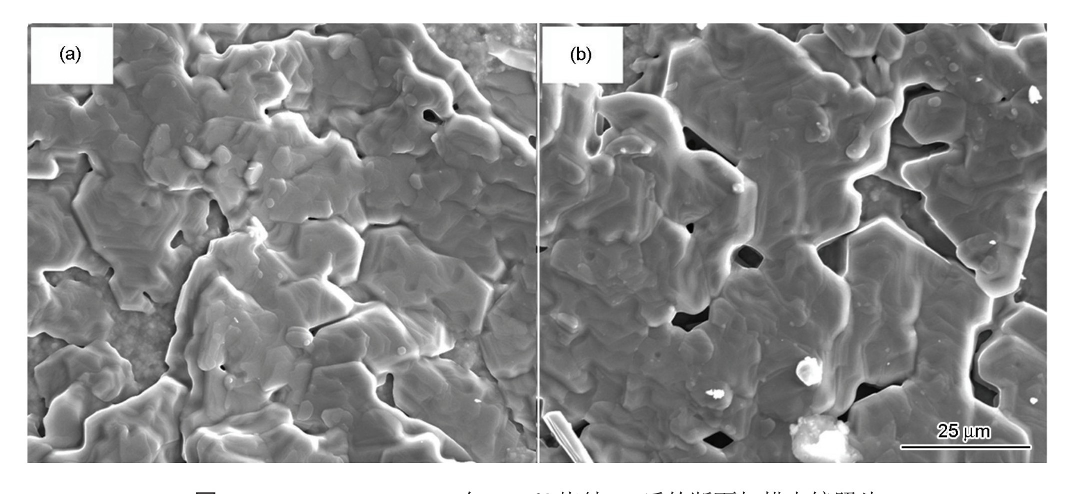
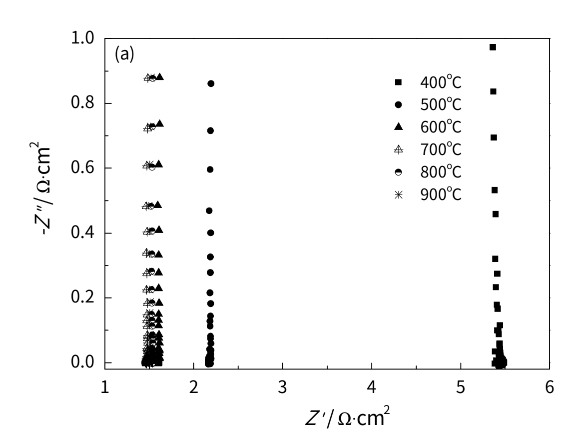


图3 $(Y_{0.08}Sr_{0.92})_{1-x}Ti_{0.6}Fe_{0.4}O_{3-\delta}$在1350℃烧结5 h后的断面扫描电镜照片

Fig.3 SEM micrographs of surface for $(Y_{0.08}Sr_{0.92})_{1-x}Ti_{0.6}Fe_{0.4}O_{3-\delta}$ (a) x=0.05 and (b) x=0.07



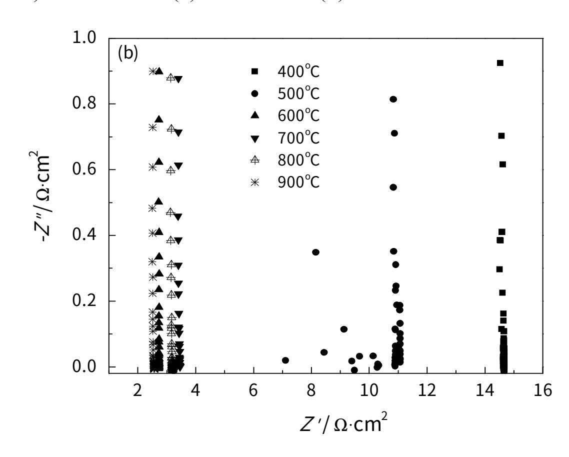


图4 $(Y_{0.08}Sr_{0.92})_{1-x}Ti_{0.6}Fe_{0.4}O_{3-\delta}$复阻抗谱图

Fig.4 Complex-plane impedance plots of the total electrical conduction at different temperatures for: (a) $(Y_{0.08}Sr_{0.92})_{0.95}Ti_{0.6}Fe_{0.4}O_{3-\delta}$; (b) $(Y_{0.08}Sr_{0.92})_{0.90}Ti_{0.6}Fe_{0.4}O_{3-\delta}$

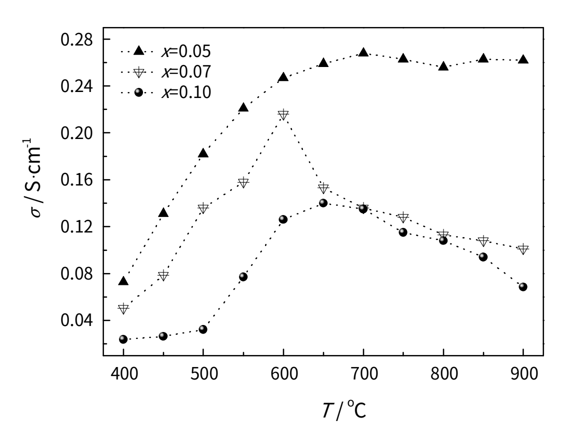
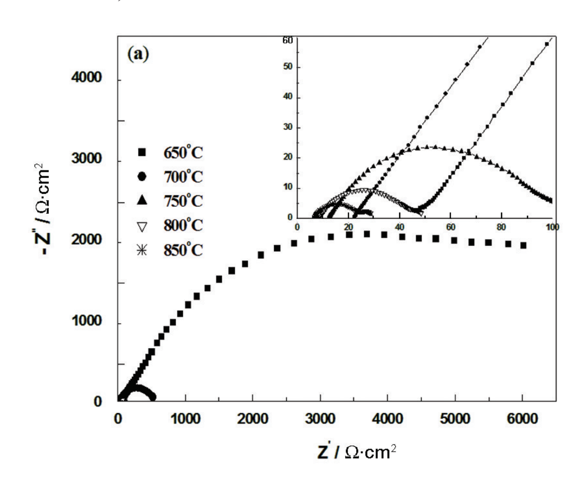


图 5 $(Y_{0.08}Sr_{0.92})_{1-x}Ti_{0.6}Fe_{0.4}O_{3-\delta}$总电导率随温度变化曲线

Fig.5 Temperature dependences of the total electrical conductivities of $(Y_{0.08}Sr_{0.92})_{1-x}Ti_{0.6}Fe_{0.4}O_{3-\delta}$ (x =0.05, 0.07, 0.10) in 400−900℃ in air



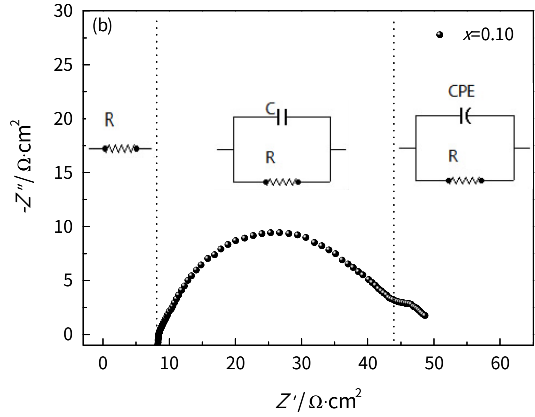
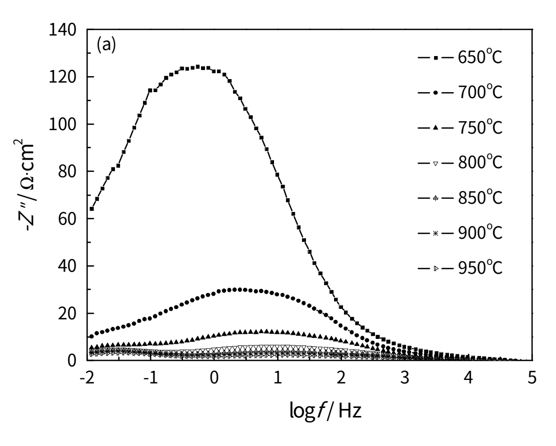
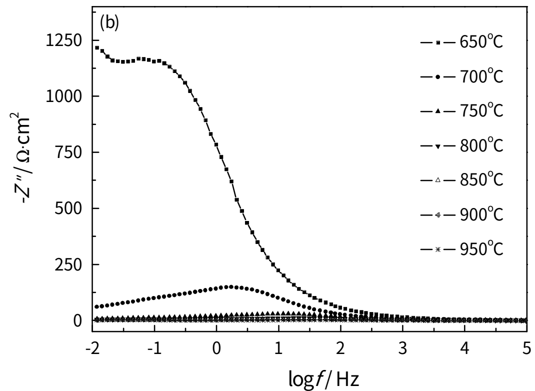


图 6 $(Y_{0.08}Sr_{0.92})_{0.90}Ti_{0.6}Fe_{0.4}O_{3-\delta}$在不同温度下离子传导的复阻抗谱图

Fig.6 Complex-plane impedance plots of the ionic conduction for $(Y_{0.08}Sr_{0.92})_{0.90}Ti_{0.6}Fe_{0.4}O_{3-\delta}$ (the inset shows the proposed equivalent circuit) (a) 650- 800℃ ; (b) 800℃

弛豫过程。随着温度的升高峰强度逐渐降低, 且峰向更高的频率移动。$(Y_{0.08}Sr_{0.92})_{0.95}Ti_{0.6}Fe_{0.4}O_{3-\delta}$在 650, 700, 750 和 800℃处的 f_{max} 分别为 0.55, 2.55, 5.49 和 11.91 Hz, 当温度继续升高时频率保持不变。在 650−950℃试样的弛豫时间为～13.4−290 ms, 说明





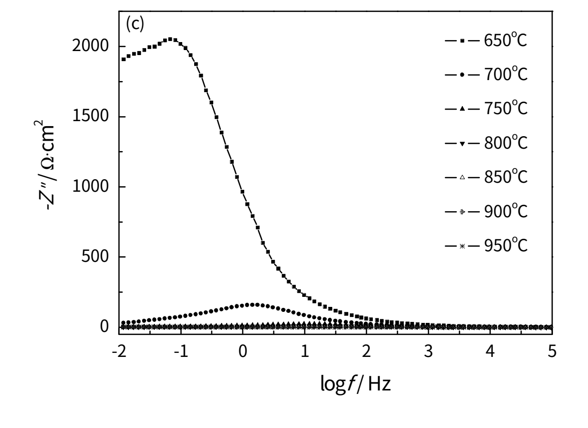


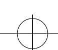
图 7 $(Y_{0.08}Sr_{0.92})_{1-x}Ti_{0.6}Fe_{0.4}O_{3-\delta}$的$-Z''$与频率的关系

Fig.7 Variation of impedance Z'' as function of frequency at $Y_{0.08}Sr_{0.92}Ti_{1-x}Fe_xO_{3-\delta}$ (a) x= 0.05, (b) x= 0.07 and (c) x=0.10

表 1 $(Y_{0.08}Sr_{0.92})_{1-x}Ti_{0.6}Fe_{0.4}O_{3-\delta}$的 f_{max} 和 τ

Table 1 f_{max} and τ of $(Y_{0.08}Sr_{0.92})_{1-x}Ti_{0.6}Fe_{0.4}O_{3-\delta}$

T \ f_{max} \ x	x=0.05	x=0.07	x=0.10
650℃	0.55Hz	0.118 Hz	0.066 Hz
700℃	2.55 Hz	1.738 Hz	1.434 Hz
750℃	5.49 Hz	11.91 Hz	11.91 Hz
800℃	11.91 Hz	21.23 Hz	21.23 Hz
τ	～13.4－290 ms	～7.5－1349 ms	～7.5－2413 ms



晶界弛豫随着温度的升高而减小。其它试样的f_{max}与τ列于表1, 可见随着A位缺位量的增大$(Y_{0.08}Sr_{0.92})_{1-x}$-$Ti_{0.6}Fe_{0.4}O_{3-\delta}$的离子传导的弛豫时间逐渐增大。

3 结 论

1. A位缺位的$(Y_{0.08}Sr_{0.92})_{1-x}Ti_{0.6}Fe_{0.4}O_{3-\delta}$的总电导率随着温度的升高先增大后减小, 表现为n型电子导电行为, 样品的总电导率随着A位缺位量的增大而减小。

2. A位缺位的$(Y_{0.08}Sr_{0.92})_{1-x}Ti_{0.6}Fe_{0.4}O_{3-\delta}$的总电导率阻抗谱只显示出高频斜线部分, 说明材料主要以电子电导为主。$(Y_{0.08}Sr_{0.92})_{1-x}Ti_{0.6}Fe_{0.4}O_{3-\delta}(x=0.05, 0.07, 0.10)$在800℃的总电导率为0.011-0.26 S•cm^{-1}, $(Y_{0.08}Sr_{0.92})_{0.95}$-$Ti_{0.6}Fe_{0.4}O_{3-\delta}$在800℃的电导率为0.162 S•cm^{-1}。

3. 随着A位缺位量的增大$(Y_{0.08}Sr_{0.92})_{1-x}Ti_{0.6}Fe_{0.4}O_{3-\delta}$的离子传导的弛豫时间逐渐增大, 说明A位缺位量的增加不利于离子在晶界中的传导。

参 考 文 献

1 Gong M., Liu X., Termbly J., Sulfur-tolerant anode materials for solid oxide fuel cell application, Journal of Power Sources, **168**(2), 289(2007)

2 Blennow P., Hagen A., Hansen K. K., Defect and electrical transport properties of Nb-doped SrTiO3, Solid State Ionics, **179**(35), 2047(2008)

3 Canales-Vazquez J., Tao S. W., Irvine J. T. S., Electrical properties in La2Sr4Ti6O19−δ: a potential anode for high temperature fuel cells, Solid State Ionics, **159**(1), 159(2003)

4 Boukamp B. A., The amazing perovskite anode, Nature Materials, **2**(5), 294(2003)

5 Li X., Zhao H., Xu N., Electrical conduction behavior of La, Co co-doped $SrTiO_3$ perovskite as anode material for solid oxide fuel cells, International Journal of Hydrogen Energy, **34**(15), 6407 (2009)

6 Li X., Zhao H., Gao F., La and Sc co-doped $SrTiO_3$ as novel anode materials for solid oxide fuel cells, Electrochemistry Communication, **10**(10), 1567(2008)

7 Litzelman S. J., Rothschild A., Tuller H. L., The electrical properties and stability of $SrTi_{0.65}Fe_{0.35}O_{3-\delta}$ thin films for auto- motive oxygen sensor applications, Sensors and Actuators B, **108**(1/2), 231 (2005)

8 Kharton V. V., Kovalevsky A. V., Viskup A. P., Transport properties and thermal expansion of $Sr_{0.97}Ti_{1-x}Fe_xO_{3-\delta}$ (x=0.2-0.8), Journal of Solid State Chemistry, **156**(2), 437(2001)

9 Hui S. Q., Petric A., Electrical conductivity of yttrium-doped $SrTiO_3$: influence of transition metal additives, Materials Research Bulletin, **37**(7), 1215(2002)

10 Yoon J. S., Yoon M. Y., Kwak C., $Y_{0.08}Sr_{0.92}Fe_xTi_{1-x}O_{3-\delta}$ perovskite for solid oxide fuel cell anodes, Materials Science and Engineering B, **177**(2), 151(2011)

11 Fagg D. P., Kharton V. V., Frade J. R., Stability and mixed ionic–electronic conductivity of (Sr, La)(Ti, Fe)$O_{3-\delta}$ perovskites, Solid State Ionics, **156**(1/2), 45(2003)

12 Hui S., Petric A., Evaluation of yttrium-doped $SrTiO_3$ as an anode for solid oxide fuel cells, Journal of European Ceramic Society, **22** (9/10), 1673(2002)

13 Fu Q. X., Mi S. B., Wessel E., Influence of sintering conditions on microstructure and electrical conductivity of yttrium-substituted $SrTiO_3$, Journal of European Ceramic Society, **28**(4), 811(2008)

14 Kurokawa H., Yang L., Jacobson C. P., Y-doped SrTiO3 based sulfur tolerant anode for solid oxide fuel cells, Journal of Power Sources, **164**(2), 510(2007)

15 Li X., Zhao H., Gao F., Synthesis and properties of Y-doped $SrTiO_3$ as anode material for SOFC, Journal of Power Sources, **166**(1), 47 (2007)

16 SHAN Ke, GUO Xingmin, Synthesis and electrical conductivity of $Y_{0.06}Sr_{0.94}Ti_{1-x}Fe_xO_{3-\delta}$ as a mixed conductor, Materials Science and Engineering of Powder Metallurgy, **18**(6), 857(2013)
(单 科, 郭兴敏, 溶胶-凝胶法制备$Y_{0.06}Sr_{0.94}Ti_{1-x}Fe_xO_{3-\delta}$混合导体材料的电性能, 粉末冶金材料科学与工程, **18**(6), 857(2013))

17 Shan K., Guo X. M., Synthesis and electrical properties of mixed-conducting $Y_xSr_{1-x}Ti_{0.7}Fe_{0.3}O_{3-\delta}$, Materials Letters, **121**, 251(2014)

18 Zhao H. L., Cheng Y. F., Xu N. S., Oxygen permeability of A-site nonstoichiometric $Ba_xCo_{0.7}Fe_{0.2}Nb_{0.1}O_{3-\delta}$ perovskite oxides, Solid State Ionics, **181**(5-7), 354(2010)

19 Liu M. F., Zhao L., Dong D. H., High sintering ability and electrical conductivity of Zn doped La(Ca)CrO_3 based interconnect ceramics for SOFCs, Journal of Power Sources, **177**(2), 451(2008)